Predictive Simulation of Guided Wave SHM with Piezoelectric Wafer Active Sensors

Victor GIURGIUTIU

Mechanical Engineering Dept., University of South Carolina
300 S. Main St., Columbia, SC 29208, USA

Keywords: piezoelectric wafer active sensors; PWAS; structural health monitoring; SHM; guided waves; nonreflective boundaries; NRB, hybrid global local; HGL; FEM; FEA

Abstract

This paper presents an overview of recent developments on predictive simulation of guided wave structural health monitoring (SHM) with piezoelectric wafer active sensor (PWAS) transducers. The predictive simulation methodology is based on the hybrid global local (HGL) concept which allows fast analytical simulation in the undamaged global field and finite element method (FEM) simulation in the local field around and including the damage. The paper reviews the main results obtained in this area by researchers of the Laboratory for Active Materials and Smart Structures (LAMSS) at the University of South Carolina, USA. The paper has four main parts: (i) presentation of the HGL analysis; (ii) analytical simulation in 1D and 2D; (iii) scatter field generation; (iv) HGL examples. The paper ends with summary, discussion, and suggestions for future work.

1 INTRODUCTION

The paper will start with a short review of the hybrid global local (HGL) approach. Then, the paper will present the methodology for analytical guided wave simulation in the global field in interaction with PWAS transmitters, PWAS receivers, and scatter sources. Both 1-D and 2-D guided wave propagation situations are separately considered. This methodology includes multi-wave-mode interaction and mode-wave-tuning for finite-size PWAS transducers as well as PWAS impedance concepts that allow the analytical simulation of mechanical wave response as a result of an electrical input applied to the PWAS transmitter and, vice-versa, the electrical signal generated by a PWAS receiver in response to an incoming mechanical wave.

The paper will continue with a presentation of the methodology for predicting the scatter field generated from the interaction between guided waves and damage. The concept of local FEM high-density high-accuracy meshing is presented. The framework for extracting the wave-damage interaction coefficients (WDIC) is presented for the fundamental A0, S0, SH0 modes. The local FEM region is extended to partially overlap with the global analytical region such that the scatter from an incoming guided wave can be captured and identified with the appropriate A0, S0, SH0 modes. Nonreflective boundaries (NRB) are used to prevent boundary reflections from the edges of the finite size FEM region.

The last part of the paper discusses examples such as the scatter of guided waves interacting with a crack in a 1-D waveguide and the scatter from a cracked rivet hole in a 2D plate. It is shown that certain frequency-wave mode combinations may facilitate detection whereas others combinations may actually impede detection.

2 HYBRID GLOBAL LOCAL (HGL) ANALYSIS

The hybrid global local (HGL) concept can be traced back to Goetschel *et al.* [1] that used finite element method (FEM) with different mesh sizes and granularity to simulate the elastic bulk wave propagation in the global domain and the interaction of waves with scatterers in the local domain. More developments of the bulk-waves HGL approach have been more recently [2] [3] reported culminating with the full-scale CIVA simulation package that has found extensive use in nuclear industry application [4] [5]. For nondestructive evaluation (NDE) and structural health monitoring (SHM) of thin-wall structures, as specific to aerospace applications, the guided-wave approach offer specific benefits over the bulk-wave approach. However, the multi-modal character of the guided waves makes such problems an order of magnitude more difficult than the bulk-wave problems. To address guided-wave NDE of aerospace structures, Mal and co-workers envisioned in the late 1990s [6] [7] a combination of closed-form analytical solution in the global domain and FEM solution in the local domain to achieve an efficient simulation of guided wave propagation and interaction with damage in thin plates. Displacement continuity and traction balance were imposed exactly at the boundary between the local FEM and global analytical domain through a colocation or equivalent approach. An HGL application to arbitrary waveguides using the semi analytical finite element (SAFE) method is described in ref. [8].

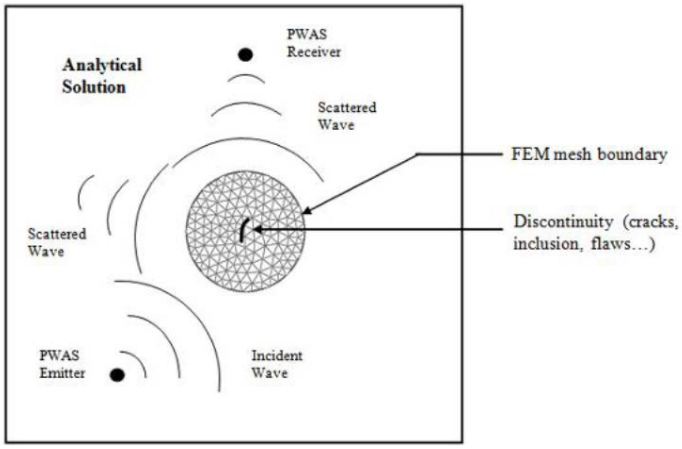

Figure 1: General 2-D set-up for Hybrid Global-Local modeling of structural sensing.

More recently, the LAMSS group extended the HGL approach to SHM applications using piezoelectric wafer active sensors (PWAS) [9]. In this approach, the guided waves are generated with a PWAS transmitter, scatter from a damage, and get picked up by a PWAS receiver (Figure 1). The travel from transmitter PWAS to the damage and from the damage to the receiver PWAS is modeled with analytical wave propagation formulae, whereas the interaction between the guided waves and the damage is done with FEM discretization [10]. As different from ref. [6] [7], the LAMSS approach to the HGL method is to replace the damage with a new guided wave source that generates the scatter field to be added to the analytical solution. The scatter field is defined in terms of wave damage interaction coefficients (WDIC) that are calculate through a local FEM analysis or by other methods.

3 ANALYTICAL GUIDED WAVE SIMULATION FOR STRAIGHT CRESTED AND CIRCULAR CRESTED GUIDED WAVES

The first step in our HGL approach was to build a simulation environment that allows for a fast and efficient modeling of the guided waves generation by a PWAS transmitter, their propagation throughout the thin-wall structure, and then their sensing by the PWAS receiver. This simulation

environment and the associate graphical user interface (GUI) has come to be know as WaveForm Revealer (WFR) [11].

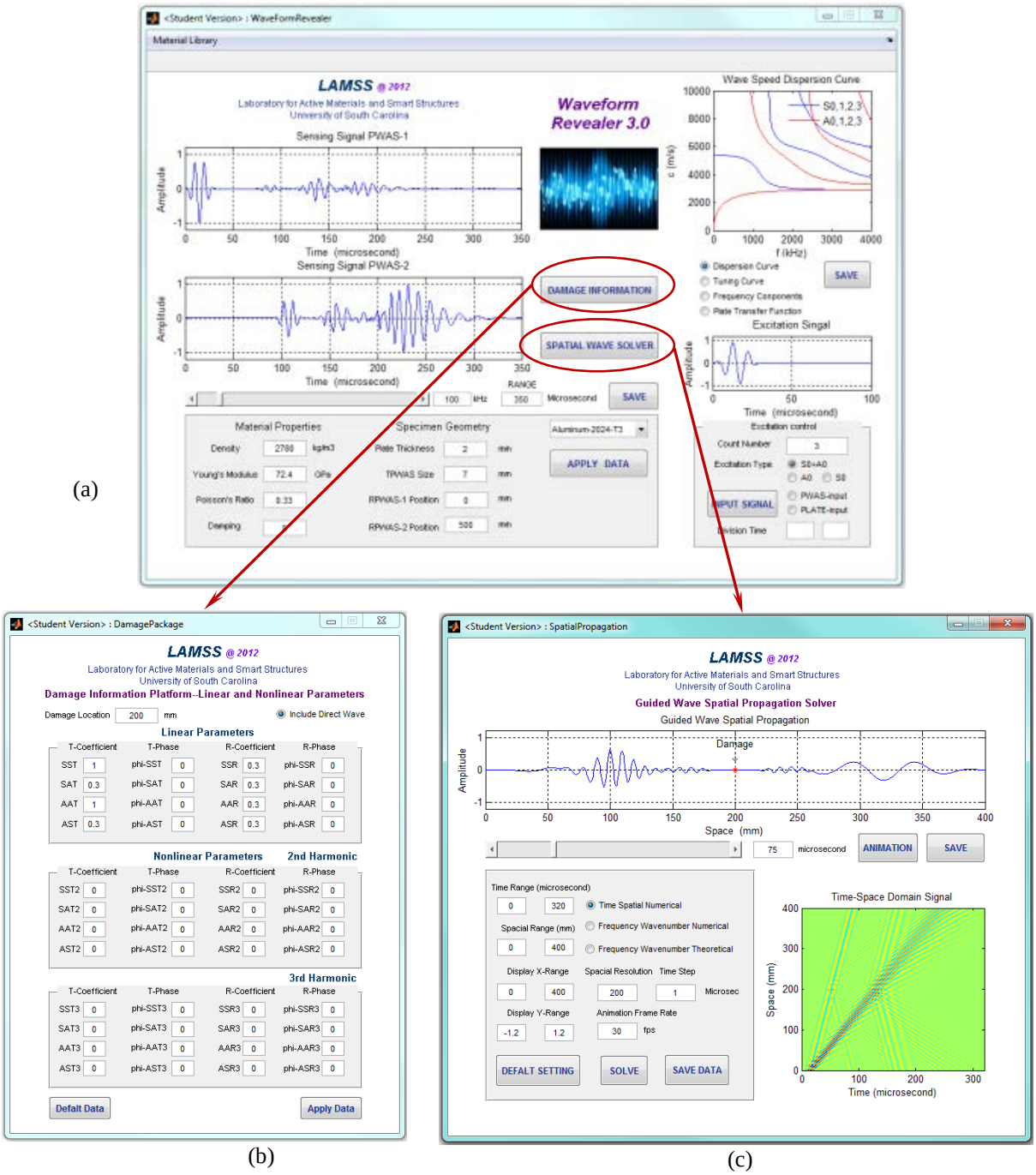

Figure 2: (a) WFR-1D GUI; (b) damage information platform; (c) guided wave spatial propagation solver

Though the guided waves are elastodynamic phenomena, their generation is done under electric excitation through the converse piezoelectric effect in the PWAS transmitter, whereas their sensing in the PWAS receiver is in the form of electric signals obtained through the direct piezoelectric effect in the PWAS transducer. Thus, the problem has a multi-physics character. In addition, the finite size of the PWAS transducers produces tuning effects, i.e., at various

frequencies, various guided wave modes may be excited or sensed differently depending on the relative ratio between their wavelength and the PWAS size (see ref. [9], Chapter 11). Besides guided wave generation, propagation, and reception, the WFR simulation environment allows for insertion of damage scatterers at user-defined locations through the use of complex-numbered WDIC values.

Two WFR GUIs have been developed, one for straight-crested guided waves (WFR-1D), the other for circular-crested guided waves (WFR-2D).

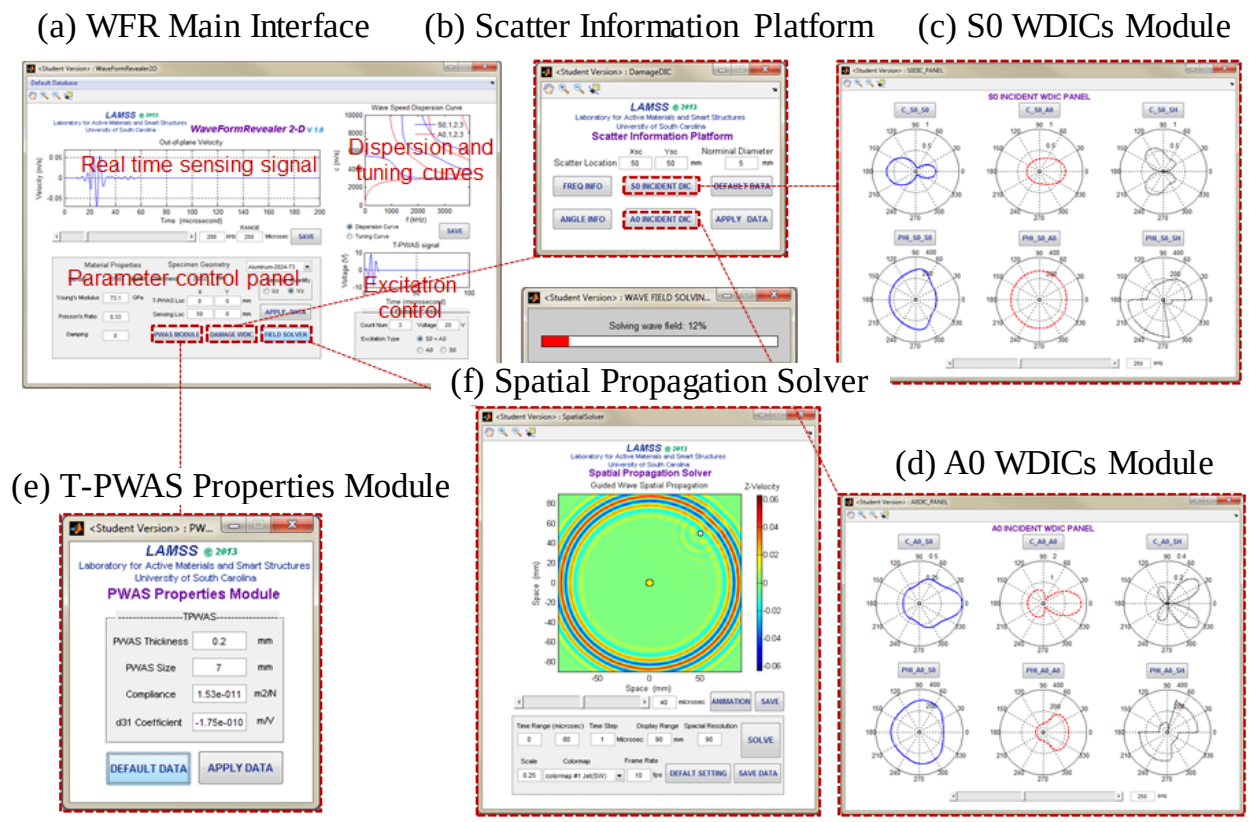

Figure 3: GUI of WFR-2D: (a) WFR-2D main interface; (b) damage information platform; (c) S0 WDICs module; (d) A0 WDICs module; (e) T-PWAS properties module; (f) spatial propagation solver.

3.1 WFR-1D

The WFR-1D assumes straight-crested guided waves, hence the problem is *y*-invariant and the wave propagation is 1D. The closed-form analytical solution of this multi-physics problem [11] was coded in MATLAB. The resulting GUI WFR-1D is shown in Figure 2a. The **spatial propagation solver** is like a B-scan. Using the analytical procedure, we obtain the time domain waveform solution at various locations along the structure. Thus, the time domain waveform solutions of a sequence of points along the wave propagation path are obtained. If we select the sequence of solution points fine enough, a time-spatial domain solution of the wave field is obtained. The spatial solution of wave field at a particular instance in time is available as shown in Figure 2b. After the time-space solution of the wave field is obtained, one can also do the frequency-wavenumber analysis to see the wave components of the signal. These will be illustrated in the case studies discussed later in this paper.

3.2 WFR-2D

The WFR-2D assumes circular-crested guided waves, hence the solution involves Bessel and Hankel functions. Figure 3a shows the WFR-2D main interface which calculates in real time the sensing signals as well as the dispersion curves and tuning curves. The parameter control panel allows users to modify host structure material properties, thickness, and transmitter-damage-sensing locations. The excitation control panel provides excitation waveform, frequency, and arbitrary excitation loading options. Users can also selectively choose the excited wave mode of interest. Figure 3b shows the damage information platform for inputting wave-damage interaction coefficients (WDICs). Figure 3c and Figure 3d show the sub-interfaces for loading S0 and A0 WDICs. The PWAS properties module allows users to define PWAS geometric and material properties (Figure 3e). The spatial propagation solver, shown in Figure 3f, iswhich calculates the transient time-space domain wave field, produces a wavefield image that can identify the damage location like a conventional ultrasonic C-scan.

4 SCATTER FIELD GENERATION

Two methods for predicting the scatter field generated by the interaction of guided waves and structural damage were explored. The first method consisted of a local FEM analysis in which nonreflective boundaries are placed on the extremities of the FEM mesh. Thus, the analysis can be performed as the damage inclusion was part of an infinite domain without unwanted reflections from the boundaries. This ensures that no standing waves are created and a pure scatter phenomenon is simulated. The second method consisted in developing an exact analytical solution of the scatter phenomenon using a series expansion onto all the propagating and nonpropagating guided wave modes present in the plate in the damage vicinity. Thus, the scatter field is generated analytically through a rapidly convergent series expansion that can be truncated to the desired accuracy.

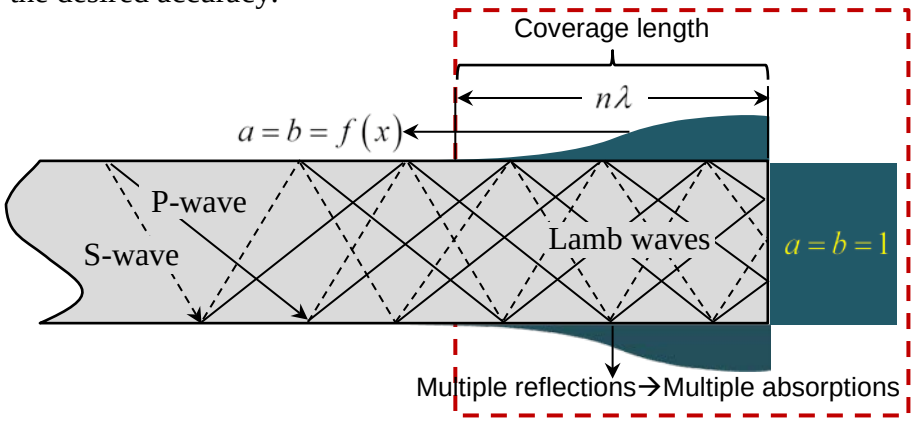

Figure 4: Extended viscous boundary on top and bottom surfaces for effective absorption of Lamb waves. The variation of coefficients a and b is described by the filled profile.

4.1 FEM WITH NONREFLECTIVE BOUNDARIES

Shen and Giurgiutiu [13] developed an NRB approach that effectively absorbs the Lamb waves at plate free edges. This concept takes into account the fact that Lamb waves result from the superposition of P and S waves that undergo multiple reflections at the top and bottom surfaces of the plate as well at the plate end (Figure 4). Hence, the NRB must inhibit both the end reflections at the plate boundary as well the top and bottom reflections in its near vicinity. In order to achieve this, viscous boundaries were added both at the plate end and on the top and bottom surfaces near the plate end; the latter viscous boundaries were smoothed out by adopting

a gradually decreasing viscosity parameter from the plate end towards the inner region. The NRB FEM analysis is done in the frequency domain such that the WDICs are generated over a wide frequency band as needed to perform the convolution with the interrogative signal generated by the transmitter PWAS.

4.2 ANALYTICAL SCATTER FIELD GENERATION WITH THE CMEP METHOD

The real, imaginary, and complex roots (wavenumbers) of the Rayleigh-Lamb equation for symmetric and antisymmetric Lamb wave modes were extracted using an efficient complex root search algorithm [14]. Thus the wave field in the vicinity of the damage was expressed as a series expansion superposition of propagating Lamb waves (real and complex wavenumbers) and evanescent Lamb waves (imaginary wavenumbers). This ensures proper representation of the wave-damage interaction phenomena, although only the non-attenuated propagating Lamb waves (real wavenumbers) would arrive at the receiver PWAS.

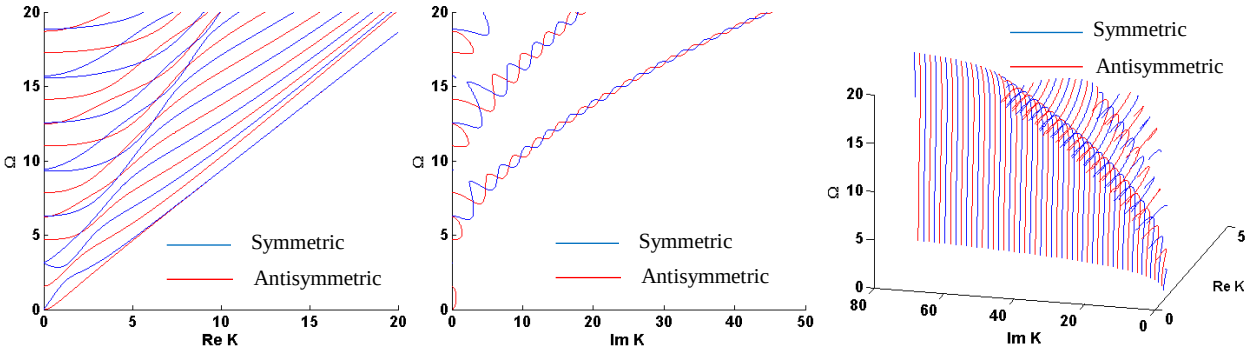

(a) (b) (c)

Figure 5: (a) real, (b) imaginary, and (c) complex roots of the Rayleigh-Lamb equation for $\nu = 0.33$

The participation factors of each of these complex waves were determined from a Galerkin solution of the boundary condition differential equations at the damage discontinuity. Fast convergence of the Galerkin approach was ensured by an appropriate vector projection which mimics the power flow expressions, i.e., the traction boundary conditions were projected onto the displacement field whereas the displacement conditions were projected onto the stress field. This approach was called complex mode expansion with vector projection (CMEP).The analytical generation of the scatter field WDIC was found to be orders of magnitude faster that the corresponding NRB FEM approach [14].

5 HGL EXAMPLES

Examples of how the HGL method can be applied to 1D and 2D problems are given next. The 1D problem considers the interaction between a straight crested wave and a notch parallel to the wavefront. A vertical crack may be simulated by a notch of vanishing width. The 2D problem considers the interaction between a circular wave front and a rivet hole experiencing a butterfly fatigue crack. Though the rivet hole itself is a wave scatterer, the presence of the butterfly crack adds additional scattering effects. By subtracting the scatter field of the hole from the scatter field of the hole with the butterfly crack, one obtains the scatter field attributable only to the butterfly crack.

5.1 1D ANALYSIS OF A NOTCH

Figure 6 shows a comparison between simulated and experimental signals resulting from a notch scatterer. The notch has a height $h_1 = 2.5$ mm and a width $d_1 = 0.25$ mm. It is machined as a long straight grove into a 3.17-mm thick 7075-T6 aluminum plate. A transmitter T-PWAS transducer is placed at 143.5 mm in front of the notch. A receiver R-PWAS transducer is placed on the other side of the notch. The wave propagation path between the T-PWAS and the R-PWAS is 303 mm. The T-PWAS is excited with a 3-count Hanning-windowed tone burst of center frequency varying from 50 kHz to 300 kHz [11]. The T-PWAS placed on top of the plate produces both S0 and A0 wave packets traveling with different group velocities. As these wave packets encounter the notch, transmission, reflection, and mode conversion takes place. Two types of experiments were performed: (a) pulse-echo; (b) pitch catch. In the pulse-echo experiment, the T-PWAS transducer acts as both transmitter and receiver. In the pitch-catch case, the T-PWAS acts as transmitter whereas the R-PWAS acts as receiver.

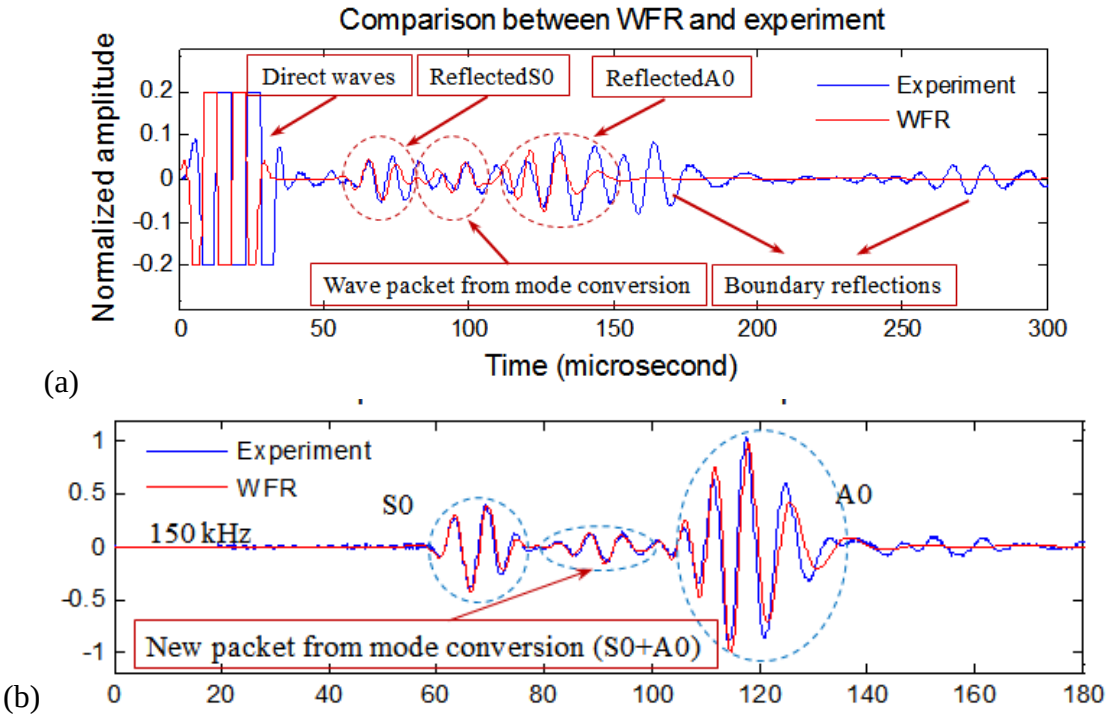

Figure 6: Comparison between WFR simulations and experiments for Lamb waves interaction with a notch: (a) pulse-echo example at 95.5 kHz; (b) pitch-catch example at 150 kHz

Figure 6a shows a pulse-echo example performed with a 95.5 kHz excitation signal. The waveform shown in Figure 6a depicts first the excitation wave (direct wave) which has a large amplitude and hence has its upper and lower peaks chopped off. The other wave packets shown in Figure 6a are the reflected S0 packet, the reflected A0 packet, and the boundary reflections. The comparison between the WFR HGL simulation and experiment reveals that the agreement with experiment is slightly better for the S0 wave than for the A0 wave. In addition, one of the boundary reflection packets superposes over the tail of the reflected A0 packet thus impeding the direct comparison with WFR predictions.

Figure 6b depicts a pitch-catch example performed at 150 kHz. In this case, the agreement between WFR HGL simulation and experiments is easier to establish because the interference

from the boundary reflections is less acute. Examination of Figure 6b reveals that the S0 wave packet is predicted almost perfectly whereas the A0 wave packed has some phase differences which may be caused by a slightly different wavespeed, possibly due to variation in the plate thickness within manufacturing tolerances. The tail of the experimental A0 wave package shows some additional wave activity which may be due boundary reflections.

5.2 2D Analysis of a Rivet Hole with Butterfly Crack

The analysis of the scatter from a butterfly crack in a rivet hole is performed in steps. For each of the S0 and A0 modes, the analysis is first performed for only a rivet hole and then for a rivet hole with butterfly cracks. For each case, i.e., undamaged and damaged, the complex scatter coefficients (WDIC) are determined at a number of frequencies of interest. Next, the "undamaged" WDICs are subtracted from the "damaged" WDICs to get the WDICs specific to the damage alone (here, the damage is the butterfly crack). For illustration, Figure 7 present a few results for the case of an incident S0 Lamb wave at a number of frequencies up to 1000 kHz.

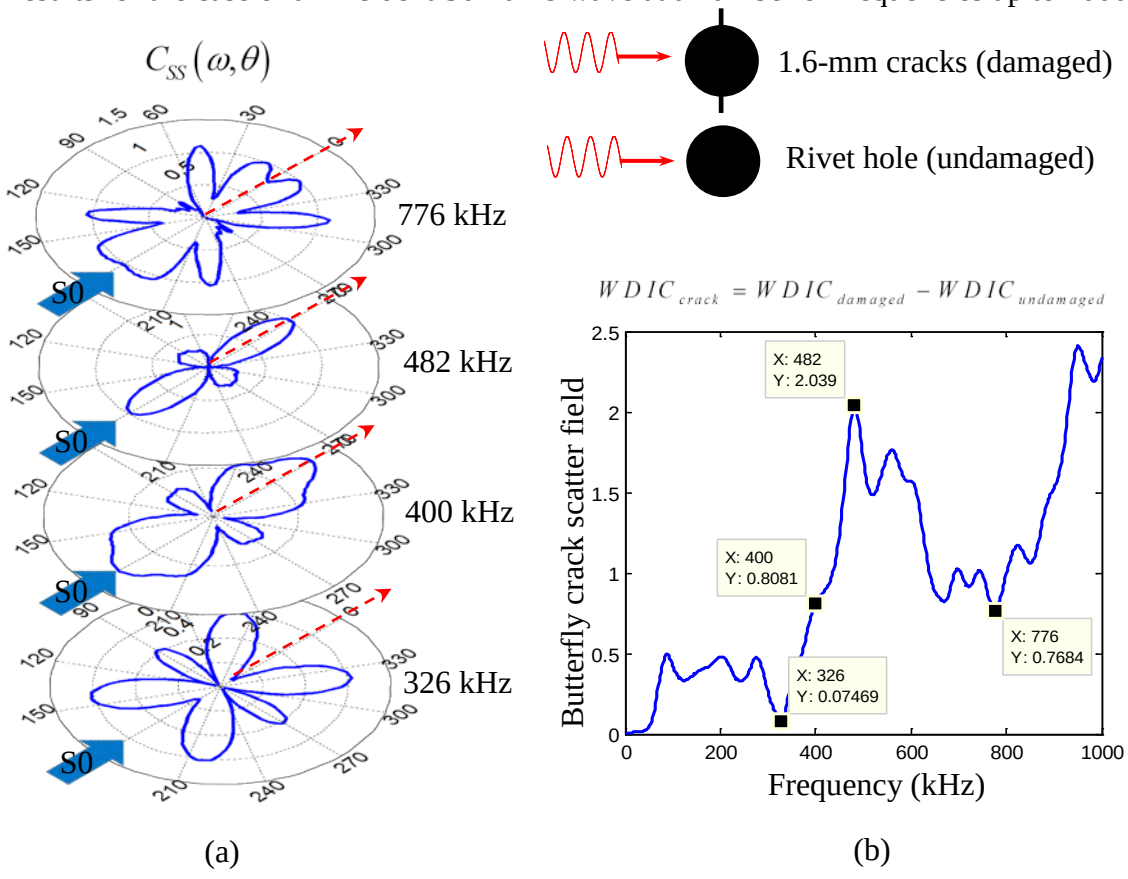

Figure 7: (a) WDIC directivity plots under various frequencies; (b) WDIC in the forward direction as a function of frequency.

Figure 7a shows the $C_{SS}(\omega,\theta)$ scattered amplitude representing the scattered S0 wave generated by an incident S0 wave. It can be observed that the scattered wave field varies azimuthally with the angle θ creating specific directivity in the polar plot. These polar plots vary dramatically with the frequency ω. In most cases, the forward facing scatter lobe seems to be the strongest. This forward direction, which is perpendicular onto the butterfly crack, is indicated by arrows in Figure 7a. However, there are frequency values for which the forward direction seems not to be

able to sense the scatter field, e.g., the 326 kHz frequency shown at the bottom of Figure 7a. When plotting the forward looking scatter field vs. frequency, we observe peaks and valleys as indicated in Figure 7b. Examination of this plot indicates that an almost zero is achieved at 326 kHz, whereas a local maximum seems to appear at 482 kHz. Similar results were obtained for the A0 incidence, but they will not be presented here for sake of brevity. For the same reason, mode conversion effects are also not presented.

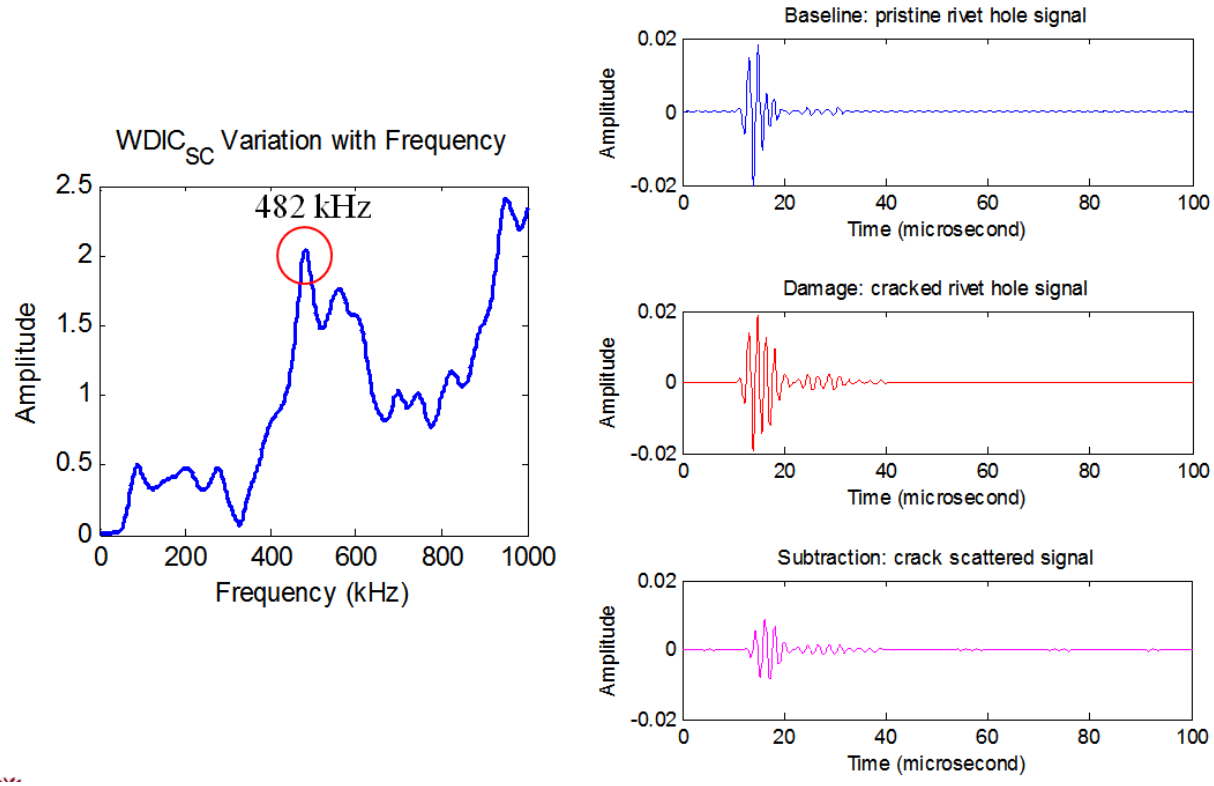

Figure 8: The crack scattered wave packet can be easily extracted when excitation is conducted at a frequency that maximizes the crack effect (here, 482 kHz)

Since, the additional scatter field due only to the butterfly crack damage is frequency dependent, the possibility of an optimal interrogation frequency arises. Figure 8 shows how the large scatter field amplitude observed at 482 kHz could be instrumental in constructing an SHM interrogation system that can easily detect the butterfly crack. As shown in the bottom right plot of Figure 8, the wave packet due to the butterfly crack alone is very strong indeed.

Also noticed in Figure 7b is the fact that certain frequencies might be inappropriate for SHM use because the scatter field would be very small, e.g., the 326 kHz frequency for which the scatter field amplitude is almost zero. However, for other damage types, or for other butterfly crack orientations and interrogating wave modes, the best detection frequency may vary and other preferred frequencies may appear.

6 SUMMARY, CONCLUSIONS, SUGGESTIONS FOR FURTHER WORK

This paper has presented a hybrid global local (HGL) method for analyzing the guided wave generation, propagation, interaction with damage, and reception during SHM with PWAS transducers. The HGL method is fast and efficient because it combines analytical solution in the global field with a local FEM solution that is small in size because it covers only the damage region and its vicinity. Both 1D and 2D situations were presented. Illustrative examples were

given in the form of 1D scatter from a notch and 2D scatter from a butterfly crack inside a rivet hole. The major conclusion of this work is that the HGL approach is highly efficient and hence recommended for the analysis of large structures in which damage has a localized nature.

Suggestions for future work include (i) further development of the CMEP method for efficient analytical determination of the scatter field; (ii) extension to the modeling of actual test coupons by the analytical introduction of boundary reflections; (iii) extension to acoustic emission studies; (iv) further development to cover guided-wave SHM of composite structures.

REFERENCES

[1] Goetschel, D.B.; Dong, S.B.; Muki, M. (1982) "A global local finite element analysis of axisymmetric scattering of elastic waves", *Journal of Applied Mechanics*, Vol. 49.

[2] Gengembre, N., Lhemery, A., Omote, R., Fouquet, T., Schumm, A. (2004) "A Semi-Analytical-FEM Hybrid Model for Simulating UT Configurations Involving Complicated Interactions of Waves with Defects", CP700 *Review of Quantitative Nondestructive Evaluation*, Vol. 23, D. O. Thompson and D. E. Chimenti (Eds.), AIP 2004, pp. 74-80

[3] Lin, S.; Yamada, H.; Fukutomi, H.; Ogata, T. (2009) "Prediction of Received Signals in Ultrasonic Testing by Finite Element Method Combined with Geometrical Optics Theory", CP1096 *Review of Quantitative Nondestructive Evaluation*, Vol. 28, D. O. Thompson and D. E. Chimenti (Eds.), AIP 2009, pp. 49-56

[4] Mahaut, S.; Lonne, S.; de Roumilly, L.; Cattiaux, G. (2006) "Validation of CIVA Simulation Tools for Ultrasonic Inspection in Realistic Configuration", *ECNDT* September 25-29, 2006, Berlin, Germany, paper We.1.4.4 http://www.ndt.net/article/ecndt2006/topic~31.htm

[5] Lonne, S.; de Roumilly, L.; LeBer, L.; Mahaut, S.; Cattiaux, G. (2006) "Experimental Validation of CIVA Ultrasonic Simulation", *5th International Conference on NDE in Nuclear Industry*, San Diego, CA, USA, May 10-12, 2006

[6] Chang, Z.; Mal, A.K. (1995) "A global local method for wave propagation across a lap joint". *Numerical methods in structural mechanics* ASME, Vol. 204, pp. 1-11

[7] Mal, A. and Chang, Z. (2000) "A semi-numerical method for elastic wave scattering calculations", Geophysical Journal International, Vol. 143, pp. 328-334.

[8] Srivastava, A. (2009) "Quantitative structural health monitoring using ultrasonic guided waves", PhD dissertation, University of California San Diego.

[9] Giurgiutiu, V. (2014) *Structural Health Monitoring with Piezoelectric Wafer Active Sensors*, 2nd Edition, Elsevier Academic Press, 1032 pages, ISBN 9780124186910, June 2014 http://store.elsevier.com/product.jsp?isbn=9780124186910

[10] Gresil, M; Giurgiutiu, V (2013) "Time-Domain Hybrid Global--Local Concept for Guided-Wave Propagation with Piezoelectric Wafer Active Sensors", *Journal of Intelligent Material Systems and Structures*, Vol. 24, No. 15, pp. 1897-1911, 2013, doi: 10.1177/1045389x13486712

[11] Shen, Y.; Giurgiutiu, V. (2014) "WaveFormRevealer: An analytical framework and predictive tool for the simulation of multi-modal guided wave propagation and interaction with damage" *Structural Health Monitoring – An International Journal*, Vol. 13, No. 5, pp. 491-511, online May 2014, doi: 10.1177/1475921714532986

[12] Shen, Y.; Giurgiutiu, V. (2016) "Combined analytical FEM approach for efficient simulation of Lamb wave damage detection", *Ultrasonics*, Vol. 69, pp. 116-128

[13] Shen, Y.; Giurgiutiu, V. (2015) "Effective non-reflective boundary for Lamb waves: theory, finite element implementation, and applications", *Wave Motion*, Vol. 58, pp. 22-41

[14] Poddar, B.; Giurgiutiu, V. (2016) "Scattering of Lamb waves from a discontinuity: An improved analytical approach", *Wave Motion*, Vol. 65 (2016), pp. 79-91